RSC Advances

PAPER

View Article Online
View Journal | View Issue

Cite this: *RSC Adv.*, 2026, **16**, 27547

Facile synthesis of (4-phenylthiophen-2-yl)methyl 1-naphthoates *via* Suzuki–Miyaura cross-coupling: anti-seizure evaluation through molecular docking, EEG analysis, and ADMET profiling

Nayab Mohsin,[ab] Nasir Rasool,[*a] Aqsa Kanwal,[a] Khaled Ahmed Saghir,[c] Imran Imran,[c] Farhan Siddique,[d] Sumaira Nadeem[de] and Muhammad Imran[fg]

This study focused on the synthesis of a novel series of (4-bromothiophen-2-yl)methyl 1-naphthoate derivatives (**5a–5h**) *via* the Suzuki–Miyaura cross-coupling with moderate to excellent yields. Acute pentylenetetrazol (PTZ) and 6 Hz psychomotor seizure models were used to investigate *in vivo* anticonvulsant effects. The **5b**, **5d**, and **5h** showed significant outcomes concerning mortality, protection, and seizure severity. In addition, the goal of the current study was to use a multifaceted strategy that integrates molecular docking (AutoDock Vina), *in silico* ADMET (SwissADME, Molsoft), and network pharmacology to explore their potential as anti-epileptic drugs against important targets (GABAA receptor (8G5G), SV2A (3O7P, 1PW4)). To find common targets, we built PPI networks and carried out functional enrichment analysis. As compared to standard medications (levetiracetam, diazepam, and PTZ), all compounds (**5a–5h**) showed greater binding affinities (−7.6 to −9.7 kcal mol^{-1}). ADMET profiles revealed drug-like characteristics with good bioavailability scores (0.55), but they also highlighted P-gp substrate liabilities and low solubility as important improvement considerations. Molsoft web server highlighted their good BBB permeation. By focusing on hub genes (SRC, AKT1, MAPK1/3, STAT3, EGFR) implicated in key signaling pathways such as PI3K-Akt, MAPK, JAK-STAT, and GABAergic synapse signaling, network analysis showed that these drugs had 15–25 targets in common with epilepsy.

Received 11th March 2026
Accepted 4th May 2026

DOI: 10.1039/d6ra02094a

rsc.li/rsc-advances

Introduction

Epilepsy is a chronic neurological condition caused by an imbalance between the excitation and inhibition of neurons and affects 1–2% of the world population. It is clinically defined by abrupt episodes that affect one or both hemispheres of the brain. Epileptic seizures may result from a transient interruption of normal brain activity.[1] Severe cases involve convulsive motor activity and protracted unconsciousness. Since the onset of symptoms typically happens before the age of ten, epilepsy has been considered a condition that affects young people for many years. However, recent data indicate that the prevalence rises with age, reaching 1.2% in the population over 85 and 0.7% in the 55–64 age range.[2] It is one of the leading causes of death with a staggering prevalence in both developing and developed nations. The expected lifetime chronicity rate for people with active epilepsy is 7.60 per 1000.[3]

Various ketogenic diets, including the classic ketogenic diet, low glycemic index treatment, medium chain triglyceride administration, and a modified Atkins diet, have been recently proposed as useful therapy in epileptic patients with pharmacoresistant epilepsy.[4] However, antiseizure medications (ASMs) remain the mainstay in epilepsy treatment. Levetiracetam, felbamate, lamotrigine, gabapentin, and topiramate are some of the novel medications that have been used to treat epilepsy. Currently, drugs available clinically produce seizure control in about 60–70% of patients. Unfortunately, about 30% of patients still experience uncontrolled seizure attacks and are considered pharmacotherapy resistant.[5] Thus, the ideal ASMs should prevent all seizure types without causing side effects that negatively impact patients' quality of life. The aforementioned factors make it imperative and vital to keep looking for safer and more potent antiepileptic medications.

[a]*Department of Chemistry, Government College University Faisalabad, Faisalabad, 38000, Pakistan. E-mail: nasirrasool@gcuf.edu.pk*
[b]*Department of Chemistry, King Fahd University of Petroleum and Minerals, Dhahran, 31261, Saudi Arabia*
[c]*Department of Pharmacology, Faculty of Pharmacy, Bahauddin Zakariya University, Multan 60800, Pakistan*
[d]*Department of Pharmaceutical Chemistry, Faculty of Pharmacy, Bahauddin Zakariya University, Multan 60800, Pakistan*
[e]*Department of Pharmacy, The Women University, Multan 60000, Pakistan*
[f]*Research Center for Advanced Materials Science (RCAMS), King Khalid University, P.O. Box 9004, Abha 61413, Saudi Arabia*
[g]*Chemistry Department, Faculty of Science, King Khalid University, P.O. Box 9004, Abha 61413, Saudi Arabia*

The main focus of our current research is on designing and synthesizing pharmacologically effective scaffolds as ASMs. With roughly seven therapeutic approvals in the past 10 years, the thiophene moiety ranks fourth among small-molecule drug approvals by the US FDA.[6] The thiophene ring is responsible for general central nervous system (CNS) depressant action and anticonvulsant activity, particularly, but the literature is scarce on its significant outcomes. The biological activities of thiophene derivatives have been found to include anti-inflammatory,[7] analgesic,[6] antidepressant,[8] antimicrobial,[9] and anticonvulsant effects. Current ASMs, including tiagabine, etizolam, and brotizolam, contain a thiophene moiety as an active pharmacophore.

Gora *et al.* evaluated the antiseizure activity of a series of pyrrolidine-2,5-dione and thiophene-based hybrid compounds in rodent models of epilepsy (psychomotor (6 Hz), maximal electroshock (MES), and PTZ seizure tests), and found **A** as a potent compound.[10] Using MES-induced seizures and PTZ models, Kulandasamy *et al.* reported the synthesis and antiseizure potential of thiophene-2,5-dicarbohydrazide derivatives and discovered (**B**) to be a potent compound.[11] Moreover, our research group also reported the synthesis of thiophen-2-ylmethyl 5-phenylfuran-2-carboxylate derivatives and found that (**C**) has anticonvulsant properties in mice using PTZ and 6 Hz psychomotor seizure models (Fig. 1).[12]

Herein, we report the synthesis of pharmacologically active (4-bromothiophen-2-yl)methyl 1-naphthoate derivatives in moderate to excellent yields *via* the Suzuki–Miyaura cross-coupling reaction, and we then investigated their antiseizure potential using the 6 Hz and PTZ mouse models. To further confirm the antiseizure potential of potent compounds, neuromuscular activity and effects on electroencephalographic (EEG) activity in the PTZ model were studied. We also incorporated integrated computational strategies to find promising hit candidates, explored their tentative multi-target mechanisms, and identified areas for structural optimization through molecular docking against key epileptic targets ($GABA_A$ and SV2A),[13] *in silico* BBB permeability analysis, drug-likeness evaluation, and network pharmacology. This would accelerate the development of next-generation epilepsy treatments.

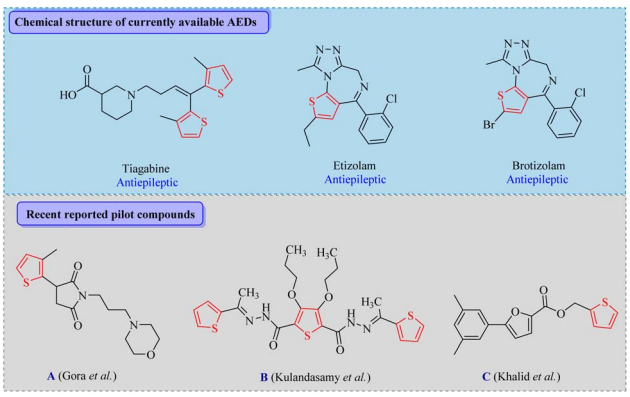

Fig. 1 Structures of ASMs and some recently reported anticonvulsant molecules bearing the thiophene moiety.

Results and discussion

Chemistry

This work is a synthetic approach for the synthesis of (4-bromothiophen-2-yl)methyl 1-naphthoate derivatives (**5a–5h**), which is based on the modification of thiophene moieties for improving their safety profiles. Naphthoic acid (**1**) was reacted with thiophene methanol (**2**) to synthesize (4-bromothiophen-2-yl)methyl 1-naphthoate (**3**) with a 90% yield. Herein, DMAP (dimethylaminopyridine) served as the catalyst, and DCC (*N*,*N*′-dicyclohexylmethanediimine) acted as the coupling agent using dichloromethane (DCM) as a solvent in the above-mentioned process, stirred at 25 °C for 18 h (Scheme 1). Notably, DCC/DMAP provides good yields with fewer side products compared to EDC/DMAP. However, solvent effects are not negligible. Different optimized conditions for this series are discussed (Table 1), and the yields reported are isolated yields obtained after the purification of synthesized compounds *via* column chromatography, where it is noted that DCM produced the maximum compound yield (**3**).

To further our investigations, we performed the Pd(0) catalyzed Suzuki reaction, which involved the formation of the corresponding (**5a–5h**) by reacting (4-bromothiophen-2-yl) methyl 1-naphthoate (**3**) with various phenyl boronic acids (**4**) (Scheme 2). This approach demonstrated exceptional functional group tolerance and achieved moderate to excellent yields (51–87%) across a wide range of substrates. Because polar solvents can interact with the palladium complex in the transition phase and usually yield better results, water (1 : 4) and 1,4-dioxane are utilized as the solvents in this coupling process.[14] One possible explanation for the enhanced yield could be the maximum solubility of aryl boronic acids in 1,4-dioxane and water.[15] Compared to their neutral counterparts, aryl boronic acids bearing electron-withdrawing groups showed decreased nucleophilicity, which resulted in delayed transmetalation, making them more vulnerable to side reactions such as homocoupling. Sterically hindered boronic acids also have lower yields because they are less available at the reaction site. It was noted that the presence of an electron-donating group caused **6h** to have the highest yield (87%), while **6e** demonstrated the lowest yield (51%) because of the existence of electron-withdrawing groups among the newly synthesized thiophene analogs.

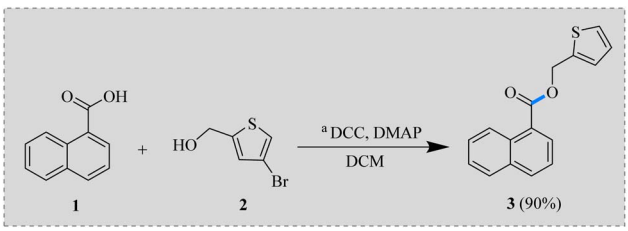

Scheme 1 Synthesis of (4-bromothiophen-2-yl)methyl 1-naphthoate (**3**). [a] Conditions: 1 (1 eq., 0.14 g, 0.725 mmol), 2 (1.1 eq., 0.137 g, 0.797 mmol), DCC (1 eq., 0.149 g, 0.725 mmol), DMAP (0.5 eq., 0.044 g, 0.3625 mmol), and DCM (20 mL), stirring for 18 h at r.t.

Table 1 (4-Bromothiophen-2-yl)methyl 1-naphthoate (**3**) % yield[a] optimization

Entry	Solvent	Catalyst	Temp.	Time (h)	% Yield
1.	THF	DMAP/DCC	40 °C	8	67
2.	THF	DMAP/EDC	40 °C	8	62
3.	Acetonitrile	DMAP/DCC	40 °C	8	15
4.	Acetonitrile	DMAP/EDC	40 °C	8	12
5.	DCM	DMAP/EDC	25 °C	18	70
6.	**DCM**	**DMAP/DCC**	**25°C**	**18**	**90**

[a] The reported isolated yields were obtained from single experiments.

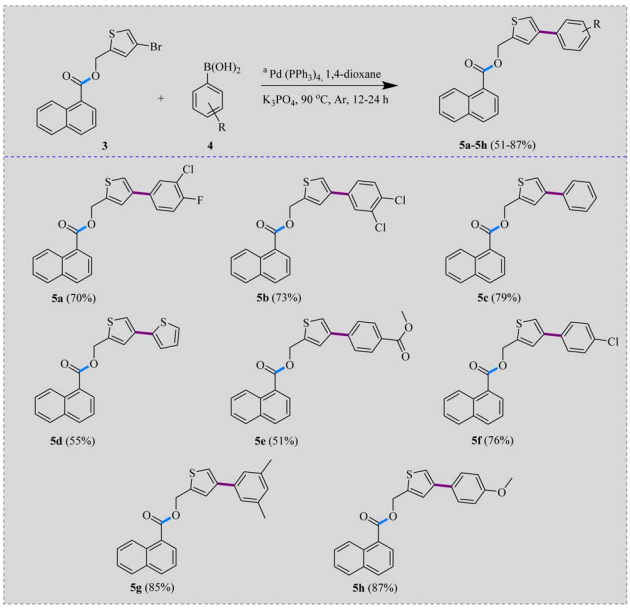

Scheme 2 Arylation of (4-bromothiophen-2-yl)methyl 1-naphthoate derivatives (**5a–5h**). [a] Conditions: **3** (1 eq., 0.2 g, 0.57 mmol), **4** (1 eq., 0.57 mmol), $Pd(PPh_3)_4$ (5 mol%, 0.028 g, 0.690 mmol), K_3PO_4 (2 eq., 0.244 g, 1.15 mmol), 1,4-dioxane/H_2O (4 : 1), 90 °C, 12–24 h under argon.

6 Hz psychomotor seizure model

Protection is defined as the absence of seizure activity within 10 seconds. Moreover, death and its delay were not applicable in this paradigm. Among the tested compounds, **5d** and **5h** produced full protection (100%), while **5b** showed partial efficacy (75%), and **5a** moderate protection (50%). **3**, **5f**, and **5g** each protected 25% of mice. **5c** and **5e** were ineffective, and no protection was observed (Table 2).

Acute PTZ seizure model

Diazepam (5 mg kg^{-1}) completely protected mice, abolishing seizures and ensuring 100% survival, while PTZ (80 mg kg^{-1}) induced rapid seizures and death, with no survival. Among tested compounds at 100 mg kg^{-1}, **5d** and **5h** significantly delayed seizure progression and improved survival (75% and 50%, respectively), while **5b** provided partial protection (50%).

Table 2 Percentage of protection against seizures induced by 6 Hz psychomotor following administration of tested compounds ($n = 4$). Mice were observed for 120 seconds after corneal stimulation

Group	Dose (mg kg^{-1})	Protected mice	Protection (%)
Levetiracetam	50	4/4	100
3	100	1/4	25
5a	100	2/4	50
5b	100	3/4	75
5c	100	0/4	0
5d	100	4/4	100
5e	100	0/4	0
5f	100	1/4	25
5g	100	1/4	25
5h	100	4/4	100

Other compounds at this dose showed minimal or no efficacy. At 150 mg kg^{-1}, **5d** and **5h** provided complete protection (100% survival), with seizure latencies similar to diazepam, while **5b** at 150 mg kg^{-1} also markedly prolonged seizure latencies and improved survival to 75% (Table 3).

EEG recordings confirmed behavioral findings observed in the acute PTZ seizure model. PTZ administration (80 mg kg^{-1}) showed progressive epileptiform discharges, including high-amplitude spike-waves corresponding to different seizure stages and death. Pretreatment with **5b**, **5d**, and **5h** at 150 mg kg^{-1} markedly attenuated seizure activity, and their EEG recordings showed delayed onset of epileptiform discharges, reduced spike frequency and amplitude, and suppression of generalized seizure patterns, resulting in survival improvement.

Neuromuscular activity assessment

Vehicle-treated mice demonstrated normal grip strength and locomotor activity. Most tested compounds (**5a**, **5b**, **5d**, **5f**, **5g**, **5h**) did not significantly alter grip strength, movement, or rearing compared with the vehicle group. In contrast, **5c** and **5e** markedly impaired neuromuscular performance, producing significant reductions in grip strength, slow movement, and slow/fast rearing, while **5a** and **5f** showed reduced fast rearing counts. Overall, the majority of compounds were well tolerated, while **5c** and **5e** exhibited clear motor toxicity at 100 mg kg^{-1} (Table 4).

Although levetiracetam achieved complete protection at 50 mg kg^{-1} in the 6 Hz psychomotor model, our synthesized thiophene–naphthoate derivatives required higher doses (100–150 mg kg^{-1}) to produce comparable efficacy. This difference can be rationalized from a chemical perspective: levetiracetam is a small, polar pyrrolidone derivative with favorable solubility and pharmacokinetics, whereas the bulky naphthoate scaffold and lipophilic thiophene ring in our compounds reduce aqueous solubility and predispose them to P-gp substrate liabilities, as highlighted in the ADMET profiling. These physicochemical features likely limit CNS exposure, demanding higher doses to achieve therapeutic concentrations. Importantly, adverse effects were systematically monitored through neuromuscular function assays (grip strength, locomotor activity, rearing counts; Table 4). Most compounds, including

Table 3 Latency to myoclonus, hindlimb extension, tonic–clonic seizures, and death were noted following PTZ (80 mg kg^{-1}) challenge in mice pretreated with diazepam, vehicle, or tested compounds (100–150 mg kg^{-1}). Values are demonstrated as mean ± SEM (n = 4). Survival (%) displays the proportion of protected mice that did not die for 30 minutes. Statistical significance *versus* PTZ control: *p < 0.05, **p < 0.01, ***p < 0.001, and ****p < 0.0001; ns, not significant

		Seizure latency (s)				
Group	Dose (mg kg^{-1})	Myoclonus	Tonic–clonic	Hindlimb extension	Death	Survival (%)
Diazepam	5	905.5 ± 301.2****	1800 ± 0.0****	1800 ± 0.0****	1800 ± 0.0****	100
PTZ	80	61.5 ± 4.4	92.2 ± 7.2	117.8 ± 13.37	131.3 ± 12.3	0
3	100	100.0 ± 7.6^{ns}	204.3 ± 76.2^{ns}	460.3 ± 208.3^{ns}	472 ± 209.4^{ns}	0
5a	100	106.4 ± 6.5^{ns}	171.3 ± 49.8^{ns}	360.5 ± 138.9^{ns}	381 ± 137.7^{ns}	0
5b	100	155.3 ± 39.2^{ns}	188.5 ± 56.5^{ns}	1374 ± 398.4**	1388 ± 394.4**	25
5c	100	75.5 ± 5.9^{ns}	106.8 ± 9.5^{ns}	124.8 ± 9.6^{ns}	137.8 ± 8.8^{ns}	0
5d	100	171.8 ± 57.0^{ns}	307.3 ± 116.6^{ns}	1102 ± 408.7*	1501 ± 298.8***	75
5e	100	71.0 ± 8.0^{ns}	102.5 ± 8.8^{ns}	118.3 ± 7.9^{ns}	130.8 ± 7.9^{ns}	0
5f	100	103.8 ± 25.7^{ns}	206.8 ± 45.7^{ns}	412.8 ± 139.5^{ns}	444.3 ± 134.6^{ns}	0
5g	100	62.7 ± 6.2^{ns}	220.8 ± 77.7^{ns}	451.5 ± 181.4^{ns}	480.8 ± 175.9^{ns}	0
5h	100	180.3 ± 92.2^{ns}	303.3 ± 127.0^{ns}	1026 ± 337.2*	1150 ± 382.1*	100
5b	150	259.0 ± 120.8^{ns}	356.3 ± 155.4***	1472 ± 328.0***	1478 ± 322.0***	75
5d	150	236.8 ± 79.4^{ns}	1159 ± 386.7**	1800 ± 0.0****	1800 ± 0.0****	100
5h	150	200.0 ± 43.6^{ns}	1062 ± 367.4****	1800 ± 0.0****	1800 ± 0.0****	100

5b, **5d**, and **5h**, did not significantly impair motor performance, indicating tolerability at the tested doses, while **5c** and **5e** produced clear motor toxicity. Thus, while compounds **5d** and **5h** demonstrated full protection at 100–150 mg kg^{-1}, their comparison with levetiracetam underscores both their promise as novel scaffolds and the need for further optimization to enhance potency and pharmacokinetic properties. The combination of these dose–response findings and the tolerability profile demonstrates the need to consider pharmacokinetic factors when combining molecular docking and ADMET predictions, since structural characteristics that may require high doses may also affect binding affinity, BBB permeability, and multi-target interactions. Although size of groups was limited to four mice per group, this design is consistent with exploratory anticonvulsant studies and ethical guidelines, as initial screening.[16,17] Despite the survival percentage and seizure latency being accepted endpoints in exploratory seizure models, EC_{50} determination remains the gold standard for quantifying drug potency. Therefore, future studies should include dose–response experiments with expanded group sizes to determine EC_{50} values, allowing direct comparison with existing ASMs.

Molecular docking

Molecular docking studies were carried out to explore the binding potential of a series of novel synthetic compounds (**3**, **5a–5h**) against the three structurally and functionally relevant targets in epilepsy *i.e.* the $GABA_A$ receptor (PDB: 8G5G), and the synaptic vesicle glycoprotein SV2A in both its inward open (PDB: 1PW4), and outward open (PDB: 3O7P) state conformations. The selected multi-target approach is crucial, as modern anti-epileptic drug discovery increasingly focuses on compounds with polypharmacological profiles to enhance efficacy and overcome drug resistance.[18] All examined compounds reflected stronger theoretical binding affinities (more negative docking scores) than the standard anti-epileptic drugs (levetiracetam (LEV), PTZ, and diazepam (DZP)) across all three chosen target proteins (Table S1). The docking scores for novel compounds ranged from −7.2 to −9.7 kcal mol^{-1}. **5e** exhibited the most

Table 4 Grip strength and locomotor activity (slow/fast movements and slow/fast rearing) were measured in mice following administration of vehicle or tested compounds (100 mg kg^{-1}). Values are demonstrated as mean ± SEM (n = 4). Statistical significance *versus* vehicle: *p < 0.05, **p < 0.01, and ****p < 0.0001; ns, not significant

		Neuromuscular activity				
Group	Dose (mg kg^{-1})	Grip strength (g)	Slow movement	Fast movement	Slow rearing	Fast rearing
Vehicle	1.0	176.2 ± 8.8	37.5 ± 5.8	52.5 ± 8.6	272.3 ± 34.9	316.8 ± 40.1
3	100	151.4 ± 7.4^{ns}	29.7 ± 4.1^{ns}	34.7 ± 5.4^{ns}	133.8 ± 30.9*	128.5 ± 23.7*
5a	100	152.7 ± 3.7^{ns}	28 ± 2.0^{ns}	47.5 ± 5.9^{ns}	224.5 ± 50.2^{ns}	215.3 ± 25.8^{ns}
5b	100	157.8 ± 6.7^{ns}	31.7 ± 5.6^{ns}	43 ± 12.8^{ns}	217.5 ± 47.2^{ns}	259.8 ± 78.5^{ns}
5c	100	96.8 ± 6.9****	17.7 ± 2.5*	23.5 ± 2.6^{ns}	121.5 ± 28.6*	100.5 ± 20.2**
5d	100	150.4 ± 6.6^{ns}	35 ± 2.7^{ns}	46.2 ± 7.7^{ns}	200 ± 23.6^{ns}	242.3 ± 52.1^{ns}
5e	100	103.1 ± 8.1****	18 ± 2.8*	30.2 ± 6.2^{ns}	114.5 ± 19.9*	130.8 ± 21.2*
5f	100	160.2 ± 14.2^{ns}	36.2 ± 6.6^{ns}	44 ± 2.3^{ns}	162 ± 23.9^{ns}	113 ± 26.8**
5g	100	153.8 ± 3.2^{ns}	32.7 ± 6.8^{ns}	50.5 ± 13.8^{ns}	206.8 ± 17.8^{ns}	258.8 ± 35.2^{ns}
5h	100	168.2 ± 11.1^{ns}	32 ± 4.5^{ns}	41.7 ± 5.4^{ns}	158.5 ± 40.5^{ns}	166 ± 38.7^{ns}

potent binding (−9.7 kcal mol^{-1}), thus, surpassing the co-crystallized ligand zolpidem (−7.0 kcal mol^{-1}) and diazepam (−6.5 kcal mol^{-1}). This is of great significance because benzodiazepines like diazepam are positive allosteric modulators of $GABA_A$, and identifying scaffolds with stronger predicted binding could lead to novel modulators.[19] **5a** has emerged as the hit candidate (−9.3 kcal mol^{-1}), far exceeding the binding score of its known ligand, levetiracetam (−5.1 kcal mol^{-1}). SV2A is the main, validated target for the standard drug levetiracetam. The superior predicted affinity of **5a** suggests it may interact with the same pocket with higher stability, potentially translating to greater potency.[20] In addition, **5b** scored the robust binding (−9.2 kcal mol^{-1}) against the SV2A (1PW4) receptor. Docking results against this inward-open conformation provide critical insights into involved interactions during various steps of the transport cycle; thus, it presented a more in-depth image of ligand-SV2A engagement.[21] Moreover, visual examination of the binding poses reflected that the studied compounds form diverse and extensive interactions within the chosen target protein's active sides, generally surpassing those of the chosen reference drugs (Table S2 and Fig. S2–S36). As far as the $GABA_A$ receptor interactions are concerned, the investigated compounds constantly involved main amino acid residues within the classical benzodiazepine site.

Like in the case of **5e** (Fig. 2), it has established an H-bond with amino acid residue THR142, which is crucial for the binding of classical benzodiazepines,[22] and a variety of π–π and π–alkyl interactions with nearby hydrophobic residues like TYR58, HIS126, and ILE227. This interaction display of **5e** (Fig. 3) imitates and outspreads compared to the chosen proteins' native co-crystallized ligand, showing a similar but potentially more robust mechanism of action. In case of the SV2A interactions, for both conformations, compounds like **5a** (Fig. 4) and **5b** (Fig. 5) formed critical hydrogen bonds with polar residues

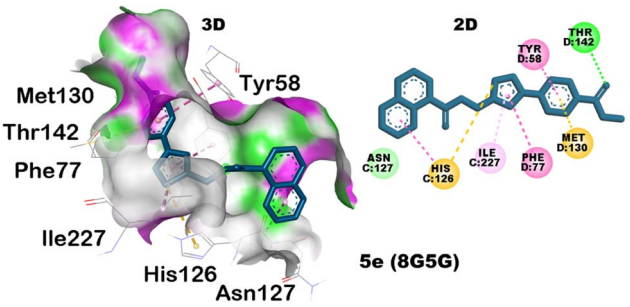

Fig. 3 3D and 2D molecular docking established interactions of **5e** with $GABA_A$ receptor (PDB ID-8G5G).

such as TYR270, GLN274, and ARG312 in the outward-open state, and TYR42, ARG45 in the inward-open state. The literature review confirms that the involved interactions with this polar network in SV2A are of key significance for high-affinity binding of anti-epileptic medications.[23] The additional halogen bonds and extensive hydrophobic interactions (*e.g.*, with TYR365 and ILE391 amino acids) observed with our compounds may be attributed to their superior predicted affinity over levetiracetam, which indicates fewer and weaker interactions in our models.

The *in vivo* experiments showed that **5d** and **5h** were the most effective compounds, furnishing 100% protection in both the tested PTZ and 6 Hz psychomotor seizure models at 100–150 mg kg^{-1}, with seizure latency data comparable to diazepam at 150 mg kg^{-1} (Table 3). This outcome is aligned with the molecular docking scores, where **5d** and **5h** displayed strong predicted binding affinities against GABA-A (8G5G: −9.1 and −8.2 kcal mol^{-1}, respectively) and SV2A in both conformational states (Table S1). At the GABA-A receptor, **5d** established a direct hydrogen bond with TYR58 (2.96 Å), a key amino acid residue

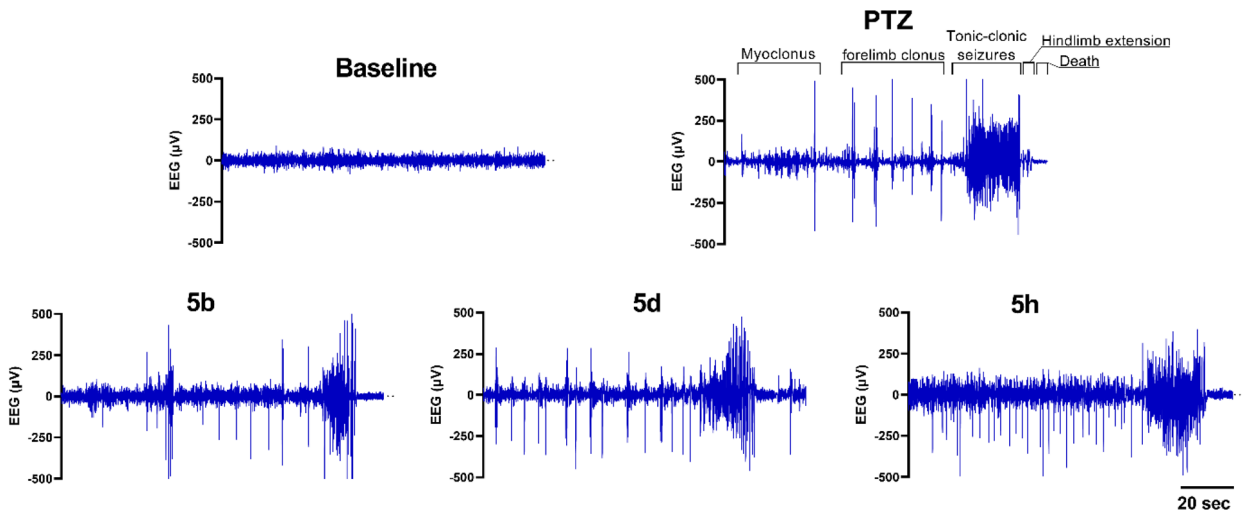

Fig. 2 Representative EEGs of 120 seconds' duration showed cortical activity in mice under baseline conditions and after PTZ (80 mg kg^{-1}) administration, following pretreatment with **5b**, **5d**, and **5h** at 150 mg kg^{-1}. PTZ showed progressive epileptiform discharges corresponding to seizure stages: myoclonus, forelimb clonus, hindlimb extension, tonic–clonic seizures, and death. In contrast, **5b**, **5d**, and **5h** attenuated seizure severity and delayed onset, with reduced spike-wave activity and improved survival.

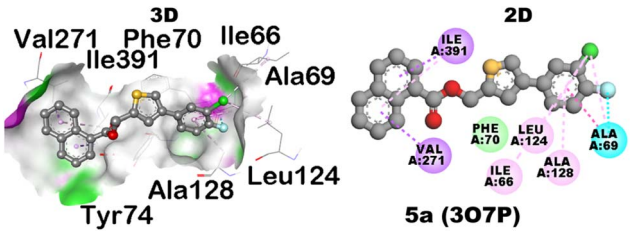

Fig. 4 3D and 2D molecular docking established interactions of **5a** with SV2A in outward open state (PDB ID: 3O7P).

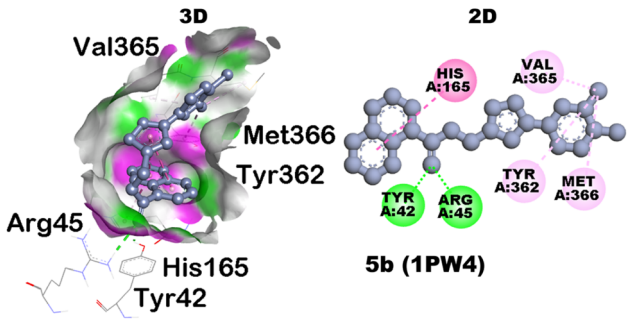

Fig. 5 3D and 2D molecular docking established interactions of **5b** with SV2A in the inward open state (PDB ID: 1PW4).

within the active binding pocket, along with additional hydrophobic contacts with TYR234 and LYS180 (Table S2 and Fig. S6). Compound **5h** involved ILE108 *via* hydrogen bond (3.62 Å) formation, along with enriched hydrophobic interactions with LEU143, VAL103, LEU145, and TRP107 (Table S2 and Fig. S9). At the SV2A receptor (3O7P), **5d** formed a hydrogen bond with ARG312 (3.37 Å), while **5h** showed an electrostatic interaction with GLU135 along with multiple hydrophobic contacts including TYR365 (Fig. S17, S21 and Table S2). At the inward-open SV2A (1PW4), **5d** formed hydrogen bonds with TYR266 and TRP161 (2.22 and 3.57 Å), while **5h** engaged PHE245 and PHE391 through hydrophobic contacts (Table S2 and Fig. S29, S33). These binding profiles, spanning both GABAergic and SV2A targets, presented a molecular basis that is consistent with the observed *in vivo* anti-seizure efficacy of these compounds.

BBB permeability

Molsoft data (Table 5) is promising, suggesting that the investigated scaffolds could be optimized for brain penetration. According to this server, all compounds are classified as moderate to good in permeation of the BBB because the (BBB) score = 6 represented high permeability and (BBB) score = 0 showed low permeation ability.[24]

Most of the investigated compounds (**3**, **5a**, **5b**, **5c**, **5d**, **5f**, **5g**, **5h**) exhibit good permeability. Compound **3** has the highest BBB value (4.82), proposing it to be the best candidate to cross the brain efficiently. On the flip side of it, **5f** scored the highest drug-likeness score (0.14) along with displaying good permeability. **5e** is the only compound that was classified as having moderate permeability with a BBB value of 3.65. It has been

Table 5 Drug likeness score and BBB permeability predicted through the web server https://molsoft.com/mprop/

Compound	Drug likeness score	BBB value	BBB interpretation
3	−0.04	4.82	Good permeability
5a	−0.04	4.16	Good permeability
5b	0.07	4.15	Good permeability
5c	−0.42	4.26	Good permeability
5d	−0.42	4.27	Good permeability
5e	−0.06	3.65	Moderate permeability
5f	0.14	4.21	Good permeability
5g	−0.41	4.18	Good permeability
5h	0.06	4.15	Good permeability

reflected that it may enter the brain less efficiently than the other compounds.

As far as the drug likeness parameter is concerned, compounds **3**, **5a**, and **5e** (−0.04 to −0.06) are very close to the threshold of being considered structurally similar to typical drugs. **5f** (0.14), **5h** (0.06), and **5b** (0.07) are the best compounds, as they are in positive values, representing that they retained the inherent features of successful commercial drugs. **5c**, **5d**, and **5g** (−0.41 to −0.42) are keeping the more negative values, as they are likely to exhibit such physical characteristic (like having too many polar groups or being too bulky) that ranks them look less like a drug as per the algorithm of this Molsoft software.

In addition, the BBB permeability computed from MolSoft established a pharmacokinetic rationale for the retrieved *in vivo* outcomes. Compounds **5d** and **5h** both revealed the BBB scores of 4.27 and 4.15, respectively, categorizing them as good BBB permeants, which shows their inherent tendency to reach the CNS at pharmacologically relevant concentrations in the mouse models. Compound **3**, although carrying only 25% protection in the 6 Hz model, carries the highest BBB score in the investigated series (4.82), encouraging it may serve as a promising lead scaffold for CNS-targeted optimization rather than a finished candidate. Compound **5e**, despite exhibiting the strongest docking score against GABA-A (−9.7 kcal mol^{-1}), showed zero *in vivo* efficacy and neuromuscular toxicity, an apparent disconnect that can be rationalized by its moderate BBB score (3.65) and significant motor impairment, suggesting that high binding affinity alone does not guarantee *in vivo* translation, and that CNS tolerability and bioavailability are equally imperative filters. Unfortunately, no experimental pharmacokinetic assay were performed in this study due to lack of availability in lab. Therefore, future studies should include direct assessment of brain/plasma concentration ratios and pharmacokinetic profiling to validate these predictions.

Network pharmacology elucidates multi-target mechanisms and hub targets

An integrated network pharmacology approach was used to unveil the possible anti-epileptic mechanisms of the investigated compounds (**5a–5h**). This network pharmacology strategy

is based on the latest model of polypharmacology in intricate and complex neurological disorders like epilepsy.[25]

It is important to note that the network pharmacology analysis presented herein is entirely computational and is intended as a hypothesis-generating framework to guide future experimental investigations, instead of serving as a claim of confirmed target engagement.

Identification of compound-disease common targets. The common genes between **5a**, **5b**, **5c**, **5d**, **5e**, **5f**, **5g**, **5h** and epilepsy are 15, 0, 0, 24, 2, 19, 5, 45 as shown in (Fig. S37–S39). These interconnecting gene pools showed that the core target ensembled through which each investigated compound group may exert its anti-epileptic effect, moving beyond approach of the individual target ($GABA_A$/SV2A) estimation in docking.

Creation and topological analysis of the protein–protein interaction (PPI) network. The common targets for all studied compounds were merged and then utilized to visualize a PPI network *via* the STRING database. The created network was fetched into Cytoscape 3.10.3 for keen analysis and visualization. The whole PPI network was composed of 90 nodes (target proteins) along with 692 edges (to reflect their key interactions). The significant topological parameters highlighted the biological relevance and high connectivity of the concerned network, as it shows the average node degree of 15.4, as well as average local clustering coefficient 0.557, along with PPI enrichment p-value $< 1.0 \times 10^{-16}$. The exceptionally low p-value reflects that the observed network has significantly more interactions than would be expected by chance for a random set of proteins of similar size, signifying that these targets are biologically connected as a functional module.

Identification of hub targets and key biological pathways. Hub targets, which are central to the network's stability and signal transduction, were identified using the cytoHubba plugin in Cytoscape by ranking nodes based on degree, betweenness centrality, and closeness centrality. The top 10 hub genes recognized are SRC, AKT1, MAPK1, MAPK3, EGFR, HRAS, STAT3, PIK3CA, PIK3R1, and JAK2 (Fig. S40 and S41). These hubs are not random but are critically involved in signaling pathways commonly implicated in epileptogenesis and neuronal excitability. SRC, MAPK1/3 (ERK1/2), and AKT1 are the core components of the PI3K-Akt and MAPK signaling pathways, which regulate neuronal survival, synaptic plasticity, and inflammatory responses, all processes dysregulated in epilepsy.[26] In addition, STAT3 and JAK2 are involved in central roles in the JAK-STAT signaling pathway, a key mediator of neuro-inflammation, as well as astrocyte reactivity in drug-resistant epilepsies.[27] EGFR and HRAS are connected with the growth factor signaling and cellular proliferation, which is associated with the malformations of cortical development, a common cause of epilepsy.

The enrichment of these specific hubs convincingly recommends that the investigated compounds may modulate epilepsy not only by direct receptor binding ($GABA_A$, SV2A) but also by inducing broader intracellular signaling cascades that control synaptic remodeling, neuronal hyperexcitability, and neuroinflammation.

Gene ontology (GO) and Kyoto encyclopedia of genes and genomes (KEGG) enrichment analysis

Based on the literature roles of these gene hubs, the compound targets are strongly predicted to be enriched in biological processes (Fig. S42) such as showing the positive regulation of kinase activity (*e.g.*, AKT, MAPK), inflammatory response and glial cell activation (STAT3, JAK2), regulation of apoptotic process and neuron death, chemical synaptic transmission and modulation of synaptic plasticity. CC analysis (Fig. S43) reveals where these interactions occur, including neuronal cell body, presynaptic membrane, somatodendritic compartment, synaptic membrane, dendrite, plasma membrane region, and axon localizations entirely consistent with CNS-active drug targets modulating synaptic transmission and neuronal firing. The localization to synapses, neuron projections, and membrane sections is consistent with targets for CNS active drugs targeting to modulate synaptic transmission as well as neuronal firing. Enrichment in Molecular Function (MF) (Fig. S44) highlights the precise biochemical activities of the target proteins, like protein kinase activity (*e.g.*, SRC, AKT1, MAPK1), transcription factor binding (*e.g.*, STAT3), receptor tyrosine kinase binding *e.g.* binding partners of EGFR, GABA receptor binding, thus validating the docking results at a systems level, voltage-gated ion channel activity as well as Tau protein kinase activity. This MF profile authorizes a mechanism involving direct modulation of neuronal signaling (kinases, ion channels) and receptor activity. KEGG pathway enrichment (Fig. S45) analysis highlighted critical signaling cascades including the PI3K-Akt signalling pathway, EGFR tyrosine kinase inhibitor resistance, and fluid shear stress and atherosclerosis pathways. The enrichment of PI3K-Akt pathway is critically implicated in neuronal survival, synaptic plasticity, and epileptogenesis, thus provides a systems-level rationale of the hub target analysis. While a direct GABAergic synapse KEGG term and at the molecular function level was not observed in these analyses, yet the GABA-A receptor engagement is supported at the cellular level by the presynaptic membrane and synaptic membrane localizations depicted in Fig. S43, providing multi-level computational evidence consistent with the *in vivo* anti-seizure outcomes.

KEGG pathway enrichment (Fig. S45) analysis pinpointed the key signaling cascades involving the PI3K-Akt signaling pathway, EGFR tyrosine kinase inhibitor resistance, and many other pathways. The enrichment in the GABAergic synapse pathway provides direct systems-level validation of the molecular docking results against the $GABA_A$ receptor. The synchronized and parallel enrichment in PI3K-Akt and MAPK pathways highlighted that an additional, complementary mechanism was probably involved in the modulation of neuro-inflammation and relevant neuronal survival, which are widely observed as key elements in epileptogenesis and drug resistance mechanisms.[28]

Construction of the compound-target-pathway network

The network pharmacology map (Fig. 6) is a comprehensive visual description of the multi-scale therapeutic approach that

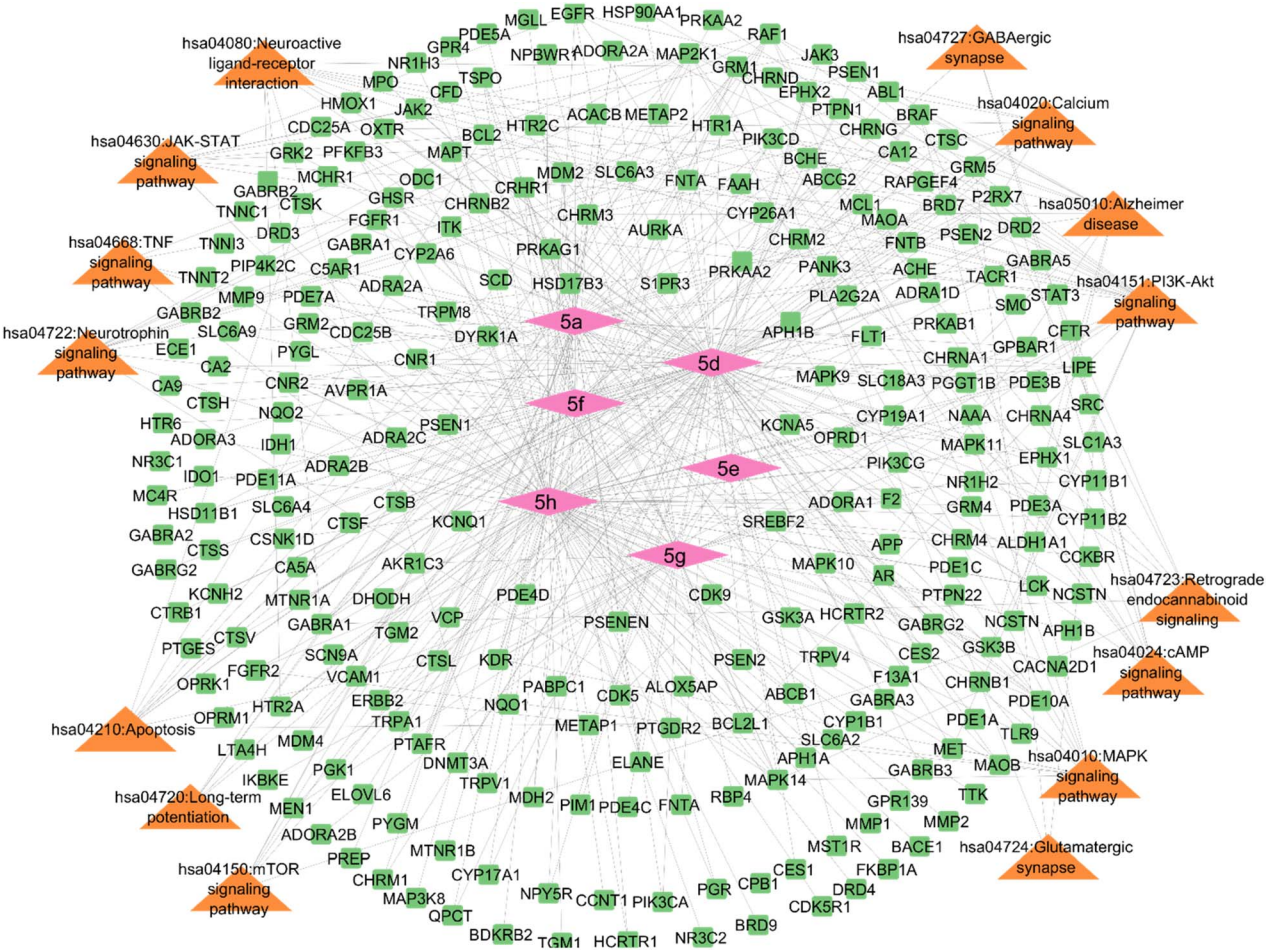

Fig. 6 The interactions among target compounds along with their pertaining target genes.

depicts the relationships between the investigated compounds, their concerned shared targets, and the engaged vital pathways. Here, the compounds **5a–5h** interacted with many target proteins, like $GABA_A$ and SV2A, which are interconnected hubs in significant pathways linked with epileptogenesis (MAPK, PI3K-Akt, *etc.*). This network, thus, showed the drug candidate's capacity to simultaneously alter multiple biological processes that are crucial to the disease, establishing a theoretical base for enhanced efficacy and probable success in complicated or resistant epileptic patients (Fig. 6).

The network pharmacology analysis identified hub targets including SRC, AKT1, MAPK1/3, EGFR, and STAT3, which are centrally involved in the PI3K-Akt, MAPK, and JAK-STAT pathways. All of which are well-documented mediators of epileptogenesis, neuroinflammation, and synaptic remodeling. Importantly, KEGG enrichment analysis also identified the GABAergic synapse pathway, providing direct systems-level corroboration of the docking results targeting GABA-A. The compounds with the highest number of common epilepsy-related gene targets, *i.e.* **5h** (44 common genes) and **5d** (24 common genes) are precisely the same compounds that performed best *in vivo* activity, reinforcing that their efficacy likely arises from a polypharmacological mechanism extending beyond single-receptor engagement.

Experimental

General remarks

The melting points of all newly synthesized compounds (**5a–5h**) were determined by using the open capillary tube method and an electrical Buchi B-540 melting-point apparatus. Shanghai Macklin Biochemical provided all the chemicals and reagents utilized in this study. The moisture- and air-sensitive reactions were performed in an inert environment. A rotary evaporator dried the synthesized compounds or reaction mixture. An Avance III Bruker spectrometer, operating at 400 MHz in deuterated solvents $CDCl_3$, was used to analyze the $^1H/^{13}C$ NMR spectra of the newly synthesized products. The coupling constant was measured in Hz, whereas the chemical shift in δppm. The progress and completion of the reaction were monitored by thin-layer chromatography (TLC) using PF254-coated cards with a pore size of 60 Å, purchased from Merck, Germany. A UV lamp emitting light in the range of 254 to 365 nm was used to detect novel derivatives of thiophene

naphthoate. Column chromatography was employed to purify the synthesized compounds (**5a–5h**).

Synthesis of (4-bromothiophen-2-yl)methyl 1-naphthoate (3). (4-Bromothiophen-2-yl)methyl 1-naphthoate was initially synthesized by the reaction of (4-bromothiophen-2-yl)methanol (1 eq., 0.14 g, 0.725 mmol) with 1-naphthoic acid (1.1 eq., 0.137 g, 0.797 mmol) in the presence of DMAP (0.5 eq., 0.044 g, 0.3625 mmol) using DCM (20 mL) as a solvent in a round-bottom flask. The cooled DCC (1 eq., 0.149 g, 0.725 mmol) was added to the above reaction mixture after 30 min of stirring at 0 °C, and it was then left to stir at room temperature for 18 h. The reaction progress was monitored *via* TLC. It underwent filtration after completion, and the solvent was removed *via* a rotary evaporator. Following that, 0.1 N HCl and EtOAc were used for acidic workup, and the product was extracted through the organic layer. The final step was to purify the desired product using column chromatography. Through spectroscopic investigation, the isolated product was verified (Scheme 1).[29,30]

Synthesis of (4-bromothiophen-2-yl)methyl 1-naphthoate derivatives (5a–5h). To an oven dried Schlenk tube containing (4-bromothiophen-2-yl)methyl 1-naphthoate (1 eq., 0.2 g, 0.57 mmol), 1,4-dioxane (7 mL), and $Pd(PPh_3)_4$ catalyst (5 mol%, 0.028 g, 0.690 mmol) were added. To ensure an inert atmosphere, the vial was purged with argon three times. Arylboronic acid (1 eq., 0.57 mmol) and K_3PO_4 (2 eq., 0.244 g, 1.15 mmol) were added to the resulting mixture after 30 min of stirring. The reaction mixture was stirred for a further 15 minutes. Subsequently, the reaction mixture was stirred at 90 °C after adding 1,4-dioxane and water (4 : 1). The progress of the reaction was monitored by TLC (Scheme 2).[31] After the completion of the reaction, it was allowed to cool at room temperature and extracted with ethyl acetate. The combined organic layers were filtered and dried over anhydrous sodium sulfate. The desired products were obtained by purifying the resultant crude product using flash column chromatography with a gradient of ethyl acetate and hexane. Standard spectroscopic techniques were used to characterize the final product.

Characterization

(4-Bromothiophen-2-yl)methyl 1-naphthoate (3). Yield 90%, pure white solid; M.P. 110–120 °C. ^{1}H NMR (400 MHz, $CDCl_3$) δ 8.92 (d, J = 8.6 Hz, 1H), 8.19 (dd, J = 7.4, 1.4 Hz, 1H), 8.02 (d, J = 8.2 Hz, 1H), 7.87 (d, J = 8.2 Hz, 1H), 7.61 (dt, J = 8.4, 4.2 Hz, 1H), 7.56–7.45 (m, 2H), 7.23 (s, 1H), 7.13 (s, 1H), 5.52 (s, 2H, CH_2). ^{13}C NMR (101 MHz, $CDCl_3$) δ 166.87 (C=O), 139.49, 133.83, 133.81, 131.39, 130.60, 130.57, 128.58, 127.96, 126.29, 126.22, 125.66, 124.45, 123.99, 109.45, 60.48 (CH_2). Elemental anal. calcd. for $C_{16}H_{11}BrO_2S$: C, 55.35; H, 3.19; S, 9.23%. Found: C, 55.38; H, 3.21; S, 9.22%.

(4-(3-Chloro-4-fluorophenyl)thiophen-2-yl)methyl 1-naphthoate (5a). Starting with **3** (1 eq., 0.2 g, 0.57 mmol), $Pd(PPh_3)_4$ catalyst (5 mol%, 0.028 g, 0.690 mmol), K_3PO_4 (2 eq., 0.244 g, 1.15 mmol), and $C_6H_5BClFO_2$ (1.0 eq., 0.099 g, 0.57 mmol), **5a** was isolated as a dark brown solid (70%); M.P. 173–180 °C. ^{1}H NMR (600 MHz, DMSO) δ 8.84 (d, J = 8.6 Hz, 1H), 8.28 (d, J = 8.2 Hz, 1H), 8.23 (dd, J = 7.2, 1.3 Hz, 1H), 8.13–8.09 (m, 2H), 8.03 (dd, J = 7.1, 2.3 Hz, 1H), 7.86 (d, J = 1.6 Hz, 1H), 7.80 (ddd, J = 8.6, 4.6, 2.3 Hz, 1H), 7.74 (ddd, J = 8.5, 6.9, 1.5 Hz, 1H), 7.71–7.66 (m, 2H), 7.53 (t, J = 9.0 Hz, 1H), 5.70 (s, 2H, CH_2). ^{13}C NMR (151 MHz, DMSO) δ 166.95 (C=O), 157.72, 156.08, 139.75, 138.96, 134.15, 133.91, 133.26, 133.23, 130.89, 130.63, 129.28, 128.50, 128.32, 128.03, 127.01, 126.98, 126.71, 125.45 (2C), 124.00, 120.58, 120.47, 117.88, 117.74, 61.55 (CH_2). Elemental anal. calcd. for $C_{22}H_{14}ClFO_2S$: C, 66.58; H, 3.56; S, 8.08%. Found: C, 66.56; H, 3.54; S, 8.07%.

(4-(3,4-Dichlorophenyl)thiophen-2-yl)methyl 1-naphthoate (5b). Starting with **3** (1 eq., 0.2 g, 0.57 mmol), $Pd(PPh_3)_4$ catalyst (5 mol%, 0.028 g, 0.690 mmol), K_3PO_4 (2 eq., 0.244 g, 1.15 mmol), and $C_6H_5BCl_2O_2$ (1.0 eq., 0.1 g, 0.57 mmol), **5b** was isolated as a light brown solid (73%); M.P. 179–183 °C. ^{1}H NMR (600 MHz, DMSO) δ 8.78 (d, J = 8.6 Hz, 1H), 8.22 (d, J = 8.2 Hz, 1H), 8.17 (dd, J = 7.3, 1.3 Hz, 1H), 8.11 (s, 1H), 8.05 (d, J = 8.1 Hz, 1H), 8.03 (d, J = 2.1 Hz, 1H), 7.83 (d, J = 1.5 Hz, 1H), 7.73 (dd, J = 8.4, 2.1 Hz, 1H), 7.70–7.66 (m, 2H), 7.62 (td, J = 7.5, 2.8 Hz, 2H), 5.64 (s, 2H, CH_2). ^{13}C NMR (151 MHz, DMSO) δ 166.95 (C=O), 139.88, 138.74, 135.90, 134.16, 133.91, 132.21, 131.50, 130.89, 130.64, 130.07, 129.28, 128.50, 128.14, 127.95, 126.98, 126.69, 126.57, 125.44 (2C), 124.72, 61.54 (CH_2). Elemental anal. calcd. for $C_{22}H_{14}Cl_2O_2S$: C, 63.93; H, 3.41; S, 7.76%. Found: C, 63.94; H, 3.43; S, 7.77%.

(4-Phenylthiophen-2-yl)methyl 1-naphthoate (5c). Starting with **3** (1 eq., 0.2 g, 0.57 mmol), $Pd(PPh_3)_4$ catalyst (5 mol%, 0.028 g, 0.690 mmol), K_3PO_4 (2 eq., 0.244 g, 1.15 mmol), and $C_6H_7BO_2$ (1.0 eq., 0.0695 g, 0.57 mmol), **5c** was isolated as a white solid (79%); M.P. 115–124 °C. ^{1}H NMR (600 MHz, DMSO) δ 8.79 (dd, J = 8.5, 1.2 Hz, 1H), 8.23 (d, J = 8.2 Hz, 1H), 8.17 (dd, J = 7.3, 1.3 Hz, 1H), 8.06 (dd, J = 8.2, 1.4 Hz, 1H), 7.93 (d, J = 1.5 Hz, 1H), 7.76 (d, J = 1.5 Hz, 1H), 7.74–7.67 (m, 3H), 7.66–7.60 (m, 2H), 7.43 (t, J = 7.8 Hz, 2H), 7.33–7.29 (m, 1H), 5.66 (s, 2H, CH_2). ^{13}C NMR (151 MHz, DMSO) δ 166.99 (C=O), 141.40, 139.44, 135.34, 134.12, 133.92, 130.89, 130.60, 129.42 (2C), 129.28, 128.48, 128.05, 127.76, 126.97, 126.78, 126.42 (2C), 125.45 (2C), 122.94, 61.66 (CH_2). Elemental anal. calcd. for $C_{22}H_{16}O_2S$: C, 76.72; H, 4.68; S, 9.31%. Found: C, 76.71; H, 4.66; S, 9.34%.

[2,3′-Bithiophen]-5′-ylmethyl 1-naphthoate (5d). Starting with **3** (1 eq., 0.2 g, 0.57 mmol), $Pd(PPh_3)_4$ catalyst (5 mol%, 0.028 g, 0.690 mmol), K_3PO_4 (2 eq., 0.244 g, 1.15 mmol), and $C_4H_5BO_2S$ (1.0 eq., 0.073 g, 0.57 mmol), **5d** was isolated as a light yellow solid (55%); M.P. 141–148 °C. ^{1}H NMR (600 MHz, DMSO) δ 8.78 (d, J = 8.6 Hz, 1H), 8.23 (d, J = 8.2 Hz, 1H), 8.17 (dd, J = 7.2, 1.3 Hz, 1H), 8.06 (dd, J = 8.1, 1.4 Hz, 1H), 7.83 (d, J = 1.5 Hz, 1H), 7.80 (dd, J = 2.9, 1.3 Hz, 1H), 7.71–7.67 (m, 2H), 7.65–7.60 (m, 3H), 7.52 (dd, J = 5.0, 1.3 Hz, 1H), 5.64 (s, 2H, CH_2). ^{13}C NMR (151 MHz, DMSO) δ 166.96 (C=O), 139.15, 137.04, 136.88, 134.12, 133.91, 130.88, 130.59, 129.28, 128.48, 128.30, 127.41, 126.97, 126.79 (2C), 125.45 (2C), 122.25, 121.00, 61.55 (CH_2). Elemental anal. calcd. for $C_{20}H_{14}O_2S_2$: C, 68.55; H, 4.03; S, 18.30%. Found: C, 68.56; H, 4.01; S, 18.34%.

(4-(4-(Methoxycarbonyl)phenyl)thiophen-2-yl)methyl 1-naphthoate (5e). Starting with **3** (1 eq., 0.2 g, 0.57 mmol), $Pd(PPh_3)_4$ catalyst (5 mol%, 0.028 g, 0.690 mmol), K_3PO_4 (2 eq., 0.244 g, 1.15 mmol), and $C_8H_9BO_4$ (1.1 eq., 0.11 g, 0.627 mmol),

5e was isolated as off white crystals (51%); M.P. 176–182 °C. ^{1}H NMR (600 MHz, DMSO) δ 8.84 (dd, J = 8.6, 1.2 Hz, 1H), 8.28 (d, J = 8.2 Hz, 1H), 8.23 (dd, J = 7.3, 1.3 Hz, 1H), 8.18 (d, J = 1.5 Hz, 1H), 8.15–8.10 (m, 1H), 8.06 (d, J = 8.4 Hz, 2H), 7.97 (d, J = 8.4 Hz, 1H), 7.94 (d, J = 8.4 Hz, 2H), 7.90 (d, J = 1.6 Hz, 1H), 7.74 (ddd, J = 8.5, 6.8, 1.5 Hz, 1H), 7.70–7.66 (m, 1H), 5.72 (s, 2H, CH_2), 3.94 (d, J = 14.1 Hz, 3H, OCH_3). ^{13}C NMR (151 MHz, DMSO) δ 166.97 (C═O), 166.44 (C═O), 140.11, 139.95, 139.69, 134.16, 133.91, 130.89, 130.63, 130.37 (2C), 129.28, 128.56, 128.50, 127.99, 127.83, 126.97, 126.71, 126.56 (2C), 125.45, 125.08, 61.57 (CH_2), 52.60 (OCH_3). Elemental anal. calcd. for $C_{24}H_{18}O_4S$: C, 71.62; H, 4.51; S, 7.97%. Found: C, 71.59; H, 4.49; S, 7.96%.

(4-(4-Chlorophenyl)thiophen-2-yl)methyl 1-naphthoate (5f). Starting with **3** (1 eq., 0.2 g, 0.57 mmol), $Pd(PPh_3)_4$ catalyst (5 mol%, 0.028 g, 0.690 mmol), K_3PO_4 (2 eq., 0.244 g, 1.15 mmol), and $C_6H_6BClO_2$ (1.0 eq., 0.089 g, 0.57 mmol), **6f** was isolated as a light brown solid (76%); M.P. 117–121 °C. ^{1}H NMR (600 MHz, DMSO) δ 8.78 (dd, J = 8.7, 1.1 Hz, 1H), 8.23 (d, J = 8.2 Hz, 1H), 8.17 (dd, J = 7.3, 1.3 Hz, 1H), 8.07–8.04 (m, 1H), 7.99 (d, J = 1.5 Hz, 1H), 7.77–7.74 (m, 3H), 7.69 (ddd, J = 8.5, 6.8, 1.4 Hz, 1H), 7.66–7.60 (m, 2H), 7.48 (d, J = 8.5 Hz, 2H), 5.65 (s, 2H, CH_2). ^{13}C NMR (151 MHz, DMSO) δ 166.97 (C═O), 140.05, 139.71, 134.19, 134.14, 133.91, 132.27, 130.89, 130.62, 129.37 (2C), 129.28, 128.49, 128.15 (2C), 127.92, 126.97, 126.73, 125.45 (2C), 123.58, 61.59 (CH_2). Elemental anal. calcd. for $C_{22}H_{15}ClO_2S$: C, 69.74; H, 3.99; S, 8.46%. Found: C, 69.72; H, 3.98; S, 8.42%.

(4-(3,5-Dimethylphenyl)thiophen-2-yl)methyl 1-naphthoate (5g). Starting with **3** (1 eq., 0.2 g, 0.57 mmol), $Pd(PPh_3)_4$ catalyst (5 mol%, 0.028 g, 0.690 mmol), K_3PO_4 (2 eq., 0.244 g, 1.15 mmol), and $C_8H_{11}BO_2$ (1.0 eq., 0.085 g, 0.57 mmol), **6g** was isolated as colorless solid (85%); M.P. 133–145 °C. ^{1}H NMR (600 MHz, DMSO) δ 8.71 (d, J = 8.6 Hz, 1H), 8.15 (d, J = 8.2 Hz, 1H), 8.09 (dd, J = 7.3, 1.4 Hz, 1H), 7.98 (d, J = 8.6 Hz, 1H), 7.78 (s, 1H), 7.64 (s, 1H), 7.61 (ddd, J = 8.6, 6.8, 1.5 Hz, 1H), 7.58–7.53 (m, 2H), 7.25 (s, 2H), 6.87 (s, 1H), 5.57 (s, 2H, CH_2), 2.24 (s, 6H, $2CH_3$). ^{13}C NMR (151 MHz, DMSO) δ 166.99 (C═O), 141.60, 139.19, 138.34, 135.18, 134.11, 133.92, 130.89, 130.59, 129.27, 129.20, 128.47, 128.18, 126.96, 126.79, 125.46, 125.43, 124.25 (2C), 122.59, 61.66 (CH_2), 21.45 (CH_3). Elemental anal. calcd. for $C_{24}H_{20}O_2S$: C, 77.39; H, 5.41; S, 8.61%. Found: C, 77.40; H, 5.39; S, 8.62%.

(4-(4-Methoxyphenyl)thiophen-2-yl)methyl 1-naphthoate (5h). Starting with **3** (1 eq., 0.2 g, 0.57 mmol), $Pd(PPh_3)_4$ catalyst (5 mol%, 0.028 g, 0.690 mmol), K_3PO_4 (2 eq., 0.244 g, 1.15 mmol), and $C_7H_9BO_3$ (1.0 eq., 0.086 g, 0.57 mmol), **5h** was isolated as a dark reddish solid (87%); M.P. 139–143 °C. ^{1}H NMR (600 MHz, DMSO) δ 8.84 (d, J = 8.6 Hz, 1H), 8.28 (d, J = 8.2 Hz, 1H), 8.23 (dd, J = 7.3, 1.3 Hz, 1H), 8.11 (d, J = 8.1 Hz, 1H), 7.84 (d, J = 1.5 Hz, 1H), 7.77–7.73 (m, 2H), 7.72–7.66 (m, 4H), 7.04 (d, J = 8.7 Hz, 2H), 5.70 (s, 2H, CH_2), 3.84 (s, 3H, OCH_3). ^{13}C NMR (151 MHz, DMSO) δ 166.99 (C═O), 159.06 (C–O), 141.16, 139.20, 134.11, 133.91, 130.88, 130.59, 129.28, 128.48, 128.09, 127.96, 127.63 (2C), 126.97, 126.80, 125.45 (2C), 121.26, 114.77 (2C), 61.68 (CH_2), 55.62 (OCH_3). Elemental anal. calcd. for $C_{23}H_{18}O_3S$: C, 73.77; H, 4.85; S, 8.56%. Found: C, 73.76; H, 4.82; S, 8.54%.

Screening for antiseizure potential

Animals. Ninety-two male C57BL/6 mice aged 6–8 weeks and weighing 22–26 g were used for experimental procedures. The animals were kept in the animal house of the Faculty of Pharmacy, Bahauddin Zakariya University (Multan, Pakistan), where they had free access to regular chow and water. The conditions under which the housing was maintained were 22–25 °C and a 12 h light/12 h dark cycle. Each animal was acclimatized to handling, the experimental room, and the apparatus. The Departmental Research Ethics Committee of the Department of Pharmacology granted approval to the research design (approval code: 02PHDS23).

Experimental procedures. Mice were randomly distributed in a series of treatment groups (n = 4 per group) to assess the antiseizure potential of synthesized compounds. One group was treated with diazepam (5 mg kg^{-1}) as a reference drug in the PTZ model, whereas another group was given PTZ (80 mg kg^{-1}) to serve as a control group. Both groups were pretreated with 1% Tween-80 about 30–45 minutes before administration of drugs. Synthesized compounds (**5a–5h**) were suspended in 1% Tween-80 and injected at a dose of 100 mg kg^{-1} 30–45 minutes before the PTZ challenge. Levetiracetam (50 mg kg^{-1}) was used in the 6 Hz psychomotor seizure model. Neuromuscular function assessment was performed before exposure to 6 Hz psychomotor or PTZ. Synthesized compounds (**5a–5h**) that showed promising protection were further subjected to electroencephalographic (EEG) monitoring at a dose of 150 mg kg^{-1}. All test compounds and reference drugs were given through the intraperitoneal route under the same conditions to maintain uniformity in the treatment groups.[32]

6 Hz psychomotor seizure model. To assess the protective effect of the synthesized compounds, a 6 Hz psychomotor seizure model was used. The 6 Hz psychomotor seizure model is a standard paradigm for evaluating treatment-resistant focal seizures, induced by corneal stimulation at 6 Hz, 0.2 ms pulse width, and 32 mA for 3 seconds. The 1% lidocaine solution was applied to each cornea before stimulation to ensure a local anesthetic effect and improve electrical conductivity. The test compounds (100 mg kg^{-1}) were injected 30–45 minutes before corneal stimulation. Immediate behavioral responses were noted, and the typical manifestations of behavior characteristic of seizures included stunned posture, Straub's tail, forelimb clonus, vibrissae twitching, grooming, and rearing. Animals were considered to be protected when they reverted to normal behavior within 10 seconds of stimulation.[33]

Acute PTZ seizure model. The PTZ model was employed to assess the synthesized compound's anticonvulsant potential, which measures latency to seizure stages and survival. It is a classical assay for generalized seizures, induced by GABAA receptor antagonism. The mice were pretreated with the test compounds (100–150 mg kg^{-1}) followed by challenge of PTZ (80 mg kg^{-1}) after a 30–45 min interval. Following PTZ treatment, mice were monitored continuously for 30 min, where

seizure progression was noted by measuring the latency of myoclonus, tonic–clonic seizure, forelimb extension, and death. The protective efficacy of the compounds was determined as survival and prolonged latency of seizures compared to the PTZ-only group.[34]

Electrode implantation and EEG recording. Mice ($n = 4$ per group) were anesthetized with intraperitoneal ketamine and xylazine, and loss of pedal withdrawal reflex was used to evaluate anesthesia depth. The mice were positioned in a stereotaxic frame (Stoelting, USA) and placed on a thermostatically controlled pad to maintain body temperature. After shaving and disinfecting the scalp with 70% ethanol, a midline incision was made, exposing and cleaning the surface of the skull. Four holes were drilled at the predetermined coordinates relative to the bregma, where tripolar cortical electrodes were implanted, and a reference screw was placed posteriorly. The electrode set was fixed using dental acrylic cement. Mice were subcutaneously injected with 0.5 mL 5% dextrose to avoid dehydration and observed until they recovered their normal feeding and locomotion. EEG experiments were performed after a recovery period of one week.[35]

Mice were individually acclimatized in transparent EEG chambers for 15–20 min, then electrodes were attached to an 8-channel bioamplifier (ADInstruments, Australia) and data digitized through PowerLab 8/35. Recording was made at a 200 Hz sample rate, low-pass filter of 60 Hz, and a time constant of 0.1 s, and analyzed with LabChart Pro software. The EEG sessions included baseline (15–20 min), compound pretreatment (30–45 min), and post-PTZ challenge (30 min), while the PTZ-only group was recorded for baseline and post-PTZ challenge.

Neuromuscular activity assessment

Grip strength test. The grip strength meter (UGO Basile S.R.L., Italy; model 47107-001) was used to test motor coordination and neuromuscular functioning. Mice were gently positioned to grasp the grid using their front paws, then pushed backward by their tails until releasing the grip, and the peak force was recorded. Each animal had given six consecutive trials separated by brief rest periods to reduce fatigue, and the average force value was considered the representative score. The experiment was performed 30 minutes following administration of compounds (100 mg kg^{-1} each) to determine possible motor impairment. Normal grip strength in comparison to vehicle controls was regarded as a sign of tolerability, whereas severe decreases indicated motor toxicity.[36]

Actimeter test. Spontaneous locomotor activity was measured with an actimeter (LE 8825, Panlab, Harvard, USA), assembled with infrared beams to detect horizontal movement and vertical rearing. Mice were acclimatized in the testing room (10–20 min), then placed individually in the actimeter for a single 5 min recording session, and the actimeter was cleaned between trials to remove olfactory cues. Recording was performed after 30 minutes of administration of compounds (100 mg kg^{-1} each) or vehicle. Each animal was observed for fast/slow movements and fast/slow rearing events, which were used as signs of spontaneous activity.[37]

Statistical analysis. Data were presented as mean ± SEM and analyzed using one-way ANOVA followed by Dunnett's post hoc test to identify differences between treatments and control. All analyses were conducted by GraphPad Prism 9.5 (San Diego, CA, USA). A p-value < 0.05 was defined as statistically significant.

Molecular docking. Molecular docking is a widely used tool to explore the ligand–receptor interaction.[38] The 3-dimensional structure of targeted receptors, $GABA_A$, SV2A, in outward open state and inward open state employing PDB ID (8G5G, 3O7P, and 1PW4),[12,39] respectively, were acquired from the RCSB database (https://www.rcsb.org/).[40] The 2-dimensional structures of the investigated compounds were sketched with the courtesy of ChemDraw 20.1.1 (ref. 41 and 42) followed by an energy minimization step by Chem3D 20.1.1.[42,43] All molecular docking calculations were carried out with AutoDockTools-1.5.7,[44,45] including the preprocessing step, for the series of these compounds with chosen receptors targeted for anti-epilepsy examination *via* docking experiment. The post-docked analysis, relevant to its corresponding target receptor, was visualized to explore the detailed binding interactions by utilizing Discovery Studio 2021 Client.[46,47] In addition, the superimposition of the docked poses with the original co-crystallized ligands showed RMSD values within an acceptable range (<2.0 Å), verifying the reliability of the docking methodology (Fig. S1).

Drug likeness and BBB permeability. Drug likeness and BBB permeability was done by utilizing MolSoft.[48]

Network pharmacology. Network pharmacology, a well-established computational method, was incorporated to examine the interactions between target drugs along with the biological system, with the intention to interpret the mechanism of action and assist the process of drug discovery.[49,50] The SwissTargetPrediction[51] was employed to identify the effective targets of these compounds and subsequently ADMET-related predictions by the SwissADME database.[52] The genes associated with epilepsy disease and common genes among the compounds were fetched from GeneCards[53] and Venny 2.1.0,[54] respectively. The STRING database[55] and Cytoscape 3.10.3 (ref. 56) were employed to construct and visualize the PPI (protein–protein interaction).

Conclusions

Palladium-catalyzed Suzuki coupling was employed to synthesize novel derivatives of (4-bromothiophen-2-yl)methyl 1-naphthoate (**5a–5h**) and were further assessed against acute PTZ and 6 Hz psychomotor models, in an effort to find improved anticonvulsive agents. The antiseizure potential of the synthesized compounds (**5a–5h**) was confirmed by the data collected after characterization, *in silico*, and *in vivo* investigations. **5d** and **5h** exhibit the most significant antiseizure potential among all compounds, in both models, compared with diazepam and levetiracetam reference drugs. Their robust potential to interact with key targets of $GABA_A$ and SV2A, depicting affinities greater than those of existing standard drugs, was revealed by

molecular docking studies. Their drug-likeness and BBB penetration suggest that these compounds (**3** and the 5-series) are tentatively robust candidates for CNS-targeted applications, as they are forecasted to cross the BBB effectively. Compound **3** could be a promising lead in relevance to brain penetration, while compound **5f** showed the nominal balance between drug-likeness and BBB permeability. Most importantly, network pharmacology explored a polypharmacological mechanism of action, linking these series to more than just receptor modification in the modulation of key epileptogenic signaling pathways (like the MAPK, PI3K-Akt, and JAK-STAT). These results support the priority of compounds such as **5a** (high SV2A affinity) and **5e** (non-P-gp substrate) for further synthetic optimization and experimental confirmation. Further research should concentrate on creating analogs with enhanced solubility and decreased P-gp efflux, followed by in-depth *in vitro* and *in vivo* testing. In addition to advancing certain epilepsy hit drugs, our current work confirms a potent integrated computational framework for the logical development of next-generation, systems-oriented neuro-therapeutic agents.

Author contributions

Writing – original draft preparation: Nayab Mohsin; writing – review and editing: Khaled Ahmed Saghir and Aqsa Kanwal; conceptualization: Imran Imran; methodology: Farhan Siddique; formal analysis and investigation: Sumaira Nadeem; resources: Farhan Siddique; project administration: Muhammad Imran; supervision: Nasir Rasool. All authors read and approved the final manuscript.

Conflicts of interest

There are no conflicts to declare.

Data availability

The data that support the findings of this study are available in the supplementary information (SI). Supplementary information: spectroscopic data for the compounds (^{1}H NMR, ^{13}C NMR) and the data supporting molecular docking and ADMET studies. See DOI: https://doi.org/10.1039/d6ra02094a.

Acknowledgements

The present data are part of the M.Phil. thesis of Nayab Mohsin. The authors gratefully acknowledge the Pakistan Council of Scientific and Industrial Research (PCSIR) (Ministry of Science and Technology), which provided financial support to access the sophisticated equipment through the data repository of the scientific instrumentation development program initiated in 2021. Furthermore, the authors are grateful to Mr Muhammad Imran, an animal house attendant, for taking care of the animals.

References

1 W. H. Abd-Allah, M. E. Aboutabl, M. N. Aboul-Enein and A. A. S. El-Azzouny, *Bioorg. Chem.*, 2017, **71**, 135–145.
2 M. Abram, A. Rapacz, S. Mogilski, G. Latacz, A. Lubelska, R. M. Kamiński and K. Kamiński, *ACS Chem. Neurosci.*, 2020, **11**, 1996–2008.
3 A. K. Sharma, E. Rani, A. Waheed and S. K. Rajput, *Journal of Epilepsy Research*, 2015, **5**, 1.
4 C. Zhou and S. Qu, *ACS Chem. Neurosci.*, 2025, **16**, 284–291.
5 D. H. Tang, D. C. Malone, T. L. Warholak, J. Chong, E. P. Armstrong, M. K. Slack, C.-H. Hsu and D. M. Labiner, *J. Clin. Neurol.*, 2015, **11**, 252–261.
6 S. Thakur, D. Kumar, S. Jaiswal, K. K. Goel, P. Rawat, V. Srivastava, S. Dhiman, H. R. Jadhav and A. R. Dwivedi, *RSC Med. Chem.*, 2025, **16**, 481–510.
7 D. H. Dawood, E. S. Nossier, M. F. Abdelhameed, G. F. Asaad and S. S. Abd El-Rahman, *Bioorg. Chem.*, 2022, **122**, 105726.
8 B. Ashalatha, B. Narayana, K. V. Raj and N. S. Kumari, *Eur. J. Med. Chem.*, 2007, **42**, 719–728.
9 S. Cakmak, S. Kansiz, M. Azam, C. C. n. Ersanlı, O. Idil, A. Veyisoglu, H. Yakan, H. Kütük and A. Chutia, *ACS Omega*, 2022, **7**, 11320–11329.
10 M. Góra, A. Czopek, A. Rapacz, A. Dziubina, M. Głuch-Lutwin, B. Mordyl and J. Obniska, *Int. J. Mol. Sci.*, 2020, **21**, 5750.
11 R. Kulandasamy, A. V. Adhikari and J. P. Stables, *Eur. J. Med. Chem.*, 2009, **44**, 3672–3679.
12 S. Khalid, A. Sabir, N. Mohsin, N. Rasool, I. Imran, F. Siddique, S. Nadeem, A. Kanwal, F. Alqahtani and M. Imran, *ChemistrySelect*, 2025, **10**, e03224.
13 B. Ashraf, N. Fatima, S. Khalid, N. Rasool, A. Kanwal, I. Imran, F. Siddique, M. Imran and M. I. Shoukat, *Chem. Biodiversity*, 2026, **23**, e01490.
14 F. Proutiere and F. Schoenebeck, *Angew. Chem., Int. Ed.*, 2011, **50**, 8192–8195.
15 H. M. Ikram, N. Rasool, M. Zubair, K. M. Khan, G. Abbas Chotana, M. N. Akhtar, N. Abu, N. B. Alitheen, A. M. Elgorban and U. A. Rana, *Molecules*, 2016, **21**, 977.
16 W. Löscher, *Neurochem. Res.*, 2017, **42**, 1873–1888.
17 E. Sitnikova, F. Onat and G. van Luijtelaar, *Frontiers in Neurology*, 2024, **15**, 1414940.
18 A. Talevi and C. Bellera, *Expert Opin. Drug Discov.*, 2024, **19**, 975–990.
19 E. Sigel and M. Ernst, *Trends Pharmacol. Sci.*, 2018, **39**, 659–671.
20 W. Löscher, M. Gillard, Z. A. Sands, R. M. Kaminski and H. Klitgaard, *CNS Drugs*, 2016, **30**, 1055–1077.
21 S. Pidathala, X. Chen, Y. Dai, L. N. Nguyen, C. Gorgulla, Y. Niu, F. Liu and C.-H. Lee, *Nat. Commun.*, 2025, **16**, 10748.
22 C. M. Borghese, M. Herman, L. D. Snell, K. J. Lawrence, H.-Y. Lee, D. S. Backos, L. A. Vanderlinden, R. A. Harris, M. Roberto and P. L. Hoffman, *Sci. Rep.*, 2017, **7**, 6230.
23 S. Dang, L. Sun, Y. Huang, F. Lu, Y. Liu, H. Gong, J. Wang and N. Yan, *Nature*, 2010, **467**, 734–738.

24 M. Gupta, H. J. Lee, C. J. Barden and D. F. Weaver, *J. Med. Chem.*, 2019, **62**, 9824–9836.
25 N. Choudhary and V. Singh, *Sci. Rep.*, 2019, **9**, 10565.
26 P. Mol, R. D. A. Balaya, S. Dagamajalu, S. Babu, P. Chandrasekaran, R. Raghavan, S. Suresh, N. Ravishankara, A. H. Raju and B. Nair, *J. Cell Commun. Signal.*, 2023, **17**, 1089–1095.
27 H. Sun, D. Ma, Y. Cheng, J. Li, W. Zhang, T. Jiang, Z. Li, X. Li and H. Meng, *Curr. Neuropharmacol.*, 2023, **21**, 2049–2069.
28 R. D. Castro-Torres, M. E. Ureña-Guerrero, L. M. Morales-Chacón, L. Lorigados-Pedre, B. Estupiñan-Díaz, L. Rocha, S. Orozco-Suárez, M. C. Rivera-Cervantes, M. Alonso-Vanegas and C. Beas-Zárate, *J. Mol. Neurosci.*, 2020, **70**, 916–929.
29 A. H. Khan, M. Bilal, A. Mahmood, N. Rasool, M. U. Qamar, M. Imran, S. I. Toma and O. Andreescu, *Pharmaceuticals*, 2024, **17**, 1241.
30 T. Maqbool, H. Younas, M. Bilal, N. Rasool, M. A. Bajaber, A. Mubarik, B. Parveen, G. Ahmad and S. A. Ali Shah, *ACS Omega*, 2023, **8**, 30306–30314.
31 M. Bilal, M. Noreen, M. U. Qamar, F. Siddique, N. Rasool and M. Imran, *RSC Adv.*, 2025, **15**, 47700–47709.
32 N. Rasool, Z. Razzaq, S. G. Khan, S. Javaid, N. Akhtar, S. Mahmood, J. B. Christensen, A. A. Altaf, S. M. M. Anjum and F. Alqahtani, *Arab. J. Chem.*, 2023, **16**, 104610.
33 M. E. Barton, B. D. Klein, H. H. Wolf and H. S. White, *Epilepsy Res.*, 2001, **47**, 217–227.
34 O. Herrera-Calderon, R. Santiváñez-Acosta, B. Pari-Olarte, E. Enciso-Roca, V. M. C. Montes and J. L. A. Acevedo, *J. Tradit. Complement. Med.*, 2018, **8**, 95–99.
35 K. A. Saghir, Z. Rehman, N. Malik, W. Ashraf, S. M. M. Anjum, R. M. Z. Mushtaq, F. Alqahtani and I. Imran, *Neurochem. Res.*, 2025, **50**, 1–12.
36 G. Bigossi, S. Marcozzi, M. E. Giuliani, G. Lai, B. Bartozzi, F. Orlando, L. Gerosa, A. M. Malvandi, D. Putavet and E. Bouma, *J. Cachexia Sarcopenia Muscle*, 2025, **16**, e70050.
37 K. A. Saghir, W. Ashraf, R. M. Z. Mushtaq, F. Alqahtani and I. Imran, *Behav. Neurol.*, 2025, **2025**, 8037864.
38 A. Laftouhi, A. Elrherabi, N. Eloutassi, F. Siddique, S. Nadeem, Z. Rais, A. Taleb, Y. A. B. Jardan, M. Bourhia and M. Taleb, *Plant Biosyst.*, 2026, **160**, 100.
39 J. Hafeez, A. Sabir, N. Rasool, U. Hafeez, F. Siddique, M. Bilal, A. Kanwal, G. Ahmad, F. Alqahtani and I. Imran, *Arab. J. Chem.*, 2024, **17**, 105889.
40 S. Bittrich, C. Bhikadiya, C. Bi, H. Chao, J. M. Duarte, S. Dutta, M. Fayazi, J. Henry, I. Khokhriakov and R. Lowe, *J. Mol. Biol.*, 2023, **435**, 167994.
41 K. Lakshmanan, H. B. Balasubramanian, R. Aiyalu and A. Ramasamy, *Res. J. Pharmacogn. Phytochem.*, 2019, **11**, 49–53.
42 A. K. Saxena, A. K. Gupta and K. S. Bhatia, *J. Math. Chem.*, 2024, **62**, 2430–2455.
43 P. Dinesha, D. Udayakumar, V. P. Shetty and V. K. Deekshit, *J. Mol. Struct.*, 2024, **1304**, 137657.
44 J. Eberhardt, D. Santos-Martins, A. F. Tillack and S. Forli, *J. Chem. Inf. Model.*, 2021, **61**, 3891–3898.
45 A. O. H. Zayed, *Discover Chemistry*, 2025, **2**, 164.
46 A. Ranjbar, S. Torabi, D. Nematollahi, M. Jamshidi and H. Ghasemi, *Infect. Dis. Rev.*, 2021, **2**, 1.
47 P. F. Ayodele, A. Bamigbade, O. O. Bamigbade, I. A. Adeniyi, E. S. Tachin, A. J. Seweje and S. T. Farohunbi, *Progress in Drug Discovery & Biomedical Science*, 2023, **6**, a0000424.
48 Y. O. Bouone, A. Bouzina and N.-E. Aouf, *Chemistry Proceedings*, 2025, **18**, 82.
49 V. Varadharajan, A. K. Balu, A. Shiju, P. Muthuramalingam, H. Shin, B. Venkidasamy, N. S. Alharbi, S. Kadaikunnan and M. Thiruvengadam, *Int. J. Med. Sci.*, 2024, **21**, 1915.
50 M. N. Anjum, S. Nadeem, M. Al-Amin, M. Saalim, F. Siddique, S. Afzal and N. Nisar, *Comput. Biol. Chem.*, 2026, **123**, 108960.
51 D. Gfeller, A. Grosdidier, M. Wirth, A. Daina, O. Michielin and V. Zoete, *Nucleic Acids Res.*, 2014, **42**, W32–W38.
52 A. Daina, O. Michielin and V. Zoete, *Sci. Rep.*, 2017, **7**, 42717.
53 Y. Tian and L. Tang, *Int. J. Clin. Exp. Pathol.*, 2022, **15**, 46.
54 H. Dong, M. Li, H. Chen, L. Tian, W. Wei, S. Wang, G. Cheng and S. Liu, *J. Cancer Res. Clin. Oncol.*, 2023, **149**, 15055–15067.
55 P. Yang, Y. Chai, M. Wei, Y. Ge and F. Xu, *Sci. Rep.*, 2023, **13**, 14114.
56 F. Wang, J.-H. Chen, B. Liu and T. Zhang, *Nat. Prod. Commun.*, 2021, **16**, 1934578X211047702.